Comparative Analysis of BEMF and Pulsating High-Frequency Current Injection Methods for PM Temperature Estimation in PMSMs

David Reigosa, *Member, IEEE*, Daniel Fernandez, Tsutomu Tanimoto, Takashi Kato, and Fernando Briz, *Senior Member, IEEE*

***Abstract*—Permanent magnet synchronous machines performance is highly dependent on the permanent magnets (PMs) temperature. However, PM temperature measurement is not easy and is not normally implemented in standard machines. Alternatively, PM temperature can be estimated. PM temperature estimation methods can be divided into three major groups: thermal model-based methods, BEMF-based methods, and methods based on the injection of some form of high-frequency signal into the stator terminals of the machine. One concern for thermal model-based methods is that the model often needs to be adjusted for each machine design and application, knowledge of the machine geometry, materials, and cooling system being, therefore, required. On the contrary, BEMF methods and methods based on high-frequency signal injection estimate the magnet temperature from measurable electrical variables, knowledge of the geometry or cooling system not being required. Though they use the same type of signals, BEMF and high-frequency signal injection methods present relevant differences. This paper realizes a comparative analysis of both methods. Physical principles, performance, and implementation will be addressed.**

***Index Terms*—High-frequency signal injection, magnet temperature estimation, permanent magnet (PM) flux linkage, permanent magnet synchronous machines (PMSMs).**

I. Introduction

DESIGN and control of PMSMs have been the focus of significant research efforts during the last three decades, mainly motivated by their superior performance and efficiency compared to other machine types [1]–[7]. However, PMSMs performance is highly dependent on the PM temperature, what have boosted the interest in the development of PM temperature measurement/estimation methods [8]–[14]. PM temperature measurement is not practical in commercial machines due to cost and robustness issues, estimation of the PM temperature being a more appealing option [8]–[11].

Manuscript received May 11, 2016; accepted July 13, 2016. Date of publication July 18, 2016; date of current version February 2, 2017. This work was supported by Nissan motor Co. Ltd., Atsugi-shi, Japan. Recommended for publication by Associate Editor R. Kennel.

D. Reigosa, D. Fernandez, and F. Briz are with the Department of Electrical, Computer & System Engineering, University of Oviedo, Gijón 33204, Spain (e-mail: diazdavid@uniovi.es; fernandezalodaniel@uniovi.es; fernando@isa.uniovi.es).

T. Tanimoto and T. Kato are with the EV System Laboratory, Nissan Research Center, Nissan Motor Co., Ltd., Atsugi-shi 243-0123, Japan (e-mail: tanimoto-t@mail.nissan.co.jp; katou-t@mail.nissan.co.jp).

Color versions of one or more of the figures in this paper are available online at http://ieeexplore.ieee.org.

Digital Object Identifier 10.1109/TPEL.2016.2592478

TABLE I
ADVANTAGES AND DISADVANTAGES OF TEMPERATURE ESTIMATION METHODS

	Thermal models	BEMF	HF signal injection
Addition signal injection	√	√	✗
Knowledge of the machine geometry and cooling system	✗	√	√
Estimation for the whole speed range, including standstill	√	✗	√
Specific calibration for each machine	✗	√	√
Previous knowledge of machine inductance maps	√	✗	√
Stator winding temperature measurement	√	✗	√
Suitable for SPMSM and IPMSM	√	√	√

PM temperature estimation methods can be divided into thermal models-based methods [12]–[13], BEMF-based methods [15]–[18], and methods that inject some form of high-frequency signal into the stator terminals of the machine [8]–[11]. Table I summarizes the intended advantages and disadvantages of each method. The major drawback of thermal models is their dependence on the geometry and cooling system of the machine, specific calibration for each machine design, and application being required. This results in large commissioning times and limited applicability. BEMF methods allow precise temperature estimation when the machine rotates at medium-high speeds, but cannot work when the machine operates at standstill or very low speed. In addition, knowledge of the machine inductance maps is needed. High-frequency signal injection methods overcome most of the limitations of BEMF methods, but require injection of an additional high-frequency signal superimposed on the fundamental excitation, which can have some adverse effects on the operation of the machine. Both BEMF and high-frequency signal injection methods need the stator winding temperature to compensate for the stator winding resistance variation. However, this is not a significant drawback in practice, as the stator winding temperature is usually measured in standard machines for protection purposes, contact type sensors being normally used.

While both BEMF and high-frequency signal injection methods are a viable option for magnet temperature estimation, they respond to radically different principles, significant differences existing, therefore, in their implementation and performance.

This paper presents a comparative analysis of BEMF and high-frequency signal injection-based temperature estimation

methods. The analysis will include accuracy, robustness, and implementation issues. The paper is organized as follows: physical principles of magnet temperature estimation using the BEMF and high-frequency signal injection are presented in Sections II and III. Sensitivity analysis for both methods is presented in Section IV. Simulation and experimental results are shown in Sections V and VI, respectively. The combined used of both methods is analyzed in Section VII, conclusion being presented in Section VII.

II. Magnet Temperature Estimation Using the BEMF

BEMF-based methods estimate the magnet temperature from the rotor PM flux linkage, which is estimated form the machine terminal voltages and currents [15]–[18].

The physical principles of the magnet temperature estimation using the BEMF can be established from the fundamental model of a PM machine in the synchronous rotor reference frame shown in (1), where $v^r_{\rm dq}$ and $i^r_{\rm dq}$ are the stator voltage and current complex vectors in the rotor synchronous reference frame, R_d, R_q, L_d, and L_q are the d- and q-axes resistances and inductances, respectively, ω_r is the machine speed, $\lambda_{\rm pm}$ is the PM flux, and p is the differential operator

$$\begin{bmatrix} v^r_d \\ v^r_q \end{bmatrix} = \begin{bmatrix} R_d & 0 \\ 0 & R_q \end{bmatrix} \begin{bmatrix} i^r_d \\ i^r_q \end{bmatrix} + p \begin{bmatrix} L_d & 0 \\ 0 & L_q \end{bmatrix} \begin{bmatrix} i^r_d \\ i^r_q \end{bmatrix} + \begin{bmatrix} 0 & -\omega_r L_q \\ \omega_r L_d & 0 \end{bmatrix} \begin{bmatrix} i^r_d \\ i^r_q \end{bmatrix} + \begin{bmatrix} 0 \\ \lambda_{\rm pm}\omega_r \end{bmatrix} \quad (1)$$

$$v^r_q = R_q i^r_q + pL_q i^r_q + \omega_r L_d i^r_d + \lambda_{pm}\omega_r \quad (2)$$

$$v^r_q = R_{q(T_s)} i^r_q + pL_{q\left(T_r, i^r_q, i^r_d\right)} i^r_q + \omega_r L_{d\left(T_r, i^r_q, i^r_d\right)} i^r_d + \lambda_{{\rm pm}(T_r)}\omega_r \quad (3)$$

$$\lambda_{{\rm pm}(T_r)} = \frac{v^r_q - \left(R_{q(T_s)} i^r_q + pL_{q\left(T_r, i^r_q, i^r_d\right)} i^r_q + \omega_r L_{d\left(T_r, i^r_q, i^r_d\right)} i^r_d\right)}{\omega_r} \quad (4)$$

$$\lambda_{{\rm pm}(T_r)} = \lambda_{{\rm pm}(T_0)}\left[1 + \beta\left(T_r - T_0\right)\right]. \quad (5)$$

The PM flux, $\lambda_{\rm pm}$, only affects to the q-axis. Therefore, only the q-axis equation is needed for the estimation of the PM flux, and consequently for temperature estimation, (2). In (2), R_q is function of the stator temperature, T_s, $\lambda_{\rm pm}$ is function of the magnet temperature, T_r, while L_d and L_q are both function of T_r and $i^r_{\rm dq}$ current. Equation (2) can, therefore, be expressed as (3), from which the PM flux can be obtained as (4).

The PM flux variation with the magnet temperature can be expressed as (5), where T_0 is the room temperature and β is the magnet flux thermal coefficient. The magnet temperature T_r is obtained from (5).

A limitation of these methods is that machine needs to be rotating [see (3)–(4)]; otherwise, no voltage is induced in the stator winding. Consequently, the method cannot work at standstill, and the errors can be inadmissible at low speeds.

Obtaining $\lambda_{\rm pm}$ from (4) when the machine is rotating and there is no current, i.e., $i^r_{\rm dq} = 0$ is relatively simple, $\lambda_{\rm pm}$ being given by (6). On the contrary, obtaining $\lambda_{\rm pm}$ when $i^r_{\rm dq} \neq 0$ is not trivial; knowledge of the stator temperature is needed to estimate the q-axis resistance variation using (7), where $\alpha_{\rm cu}$ is the copper thermal resistive coefficient. Also, previous knowledge of d- and q-axes inductance maps is needed (i.e., variation of the d- and q-axes inductance with $i^r_{\rm dq}$), to compensate their effect in (3)–(4) [15]–[18]

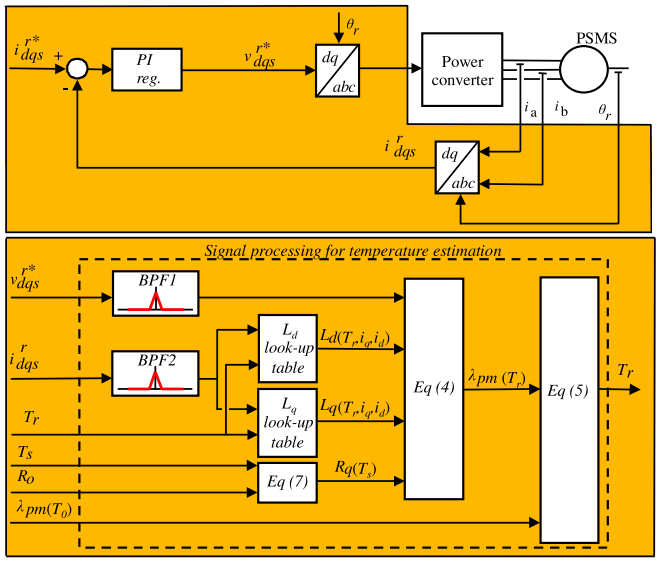

Fig. 1. Implementation using the BEMF. (top) Power converter control and (bottom) signal processing.

$$\lambda_{{\rm pm}(T_r)} = \frac{v^r_q}{\omega_r} \quad (6)$$

$$R_{q(T_s)} = R_{q(T_0)}\left[1 + \alpha_{\rm cu}\left(T_s - T_0\right)\right]. \quad (7)$$

While the use of nominal machine parameters is possible [18], it can result in significant errors as they can change with load and temperature. Alternatively, online parameters estimation methods can be used [15], [17], [18]. Furthermore, variation of the magnet temperature T_r will induce variations in both the d- and q-axes inductances and in the PM flux.

Fig. 1 shows the inverter control and signal processing block diagram for temperature estimation using the BEMF. The inputs to the temperature estimation block are the output voltage of the fundamental current controller $v^{r*}_{\rm dqs}$, the actual fundamental current $i^r_{\rm dqs}$, the estimated magnet temperature T_r, the measured stator temperature T_s, and the stator resistance at the room temperature R_0. Two band pass filters (BPF1 and BPF2 in Fig. 1) are used to eliminate high-frequency components of the fundamental voltage and current. The q-axis resistance $R_{q(T_s)}$ is obtained from (7). Two lookup tables containing estimates of the d- and q-axes inductances ($L_{d(T_r, i^r_q, i^r_d)}$ and $L_{q(T_r, i^r_q, i^r_d)}$) are used to implement (4), from which the PM flux linkage $\lambda_{{\rm pm}(T_r)}$ is obtained. The magnet temperature is eventually obtained using (5).

III. Magnet Temperature Estimation Using a High-Frequency Signal Injection

High-frequency signal injection methods estimate the magnet temperature based on the variation of the magnet high-frequency electrical resistance with temperature. The injected

high-frequency signals can be either a current or a voltage, three different waveforms have already been proposed and analyzed in the literature:

1) *Rotating voltage [8]–[9]*: it results in a relatively simple implementation, as the inverter feeding the machine is a voltage source. Unfortunately, it is only suitable for SPMSM, the estimation being sensitive to *d*- and *q*-axes inductances (L_d and L_q) variations, being also affected by the machine speed [11].
2) *Pulsating d-axis current [11]*: its implementation is more difficult than the rotating voltage injection. However, it is suitable both for SPMSM and IPMSM. In addition, it is insensitive to the speed, L_d and L_q inductance variations. Consequently, this method can be objectively considered superior to rotating voltage injection.
3) *Pulsating d-axis voltage and q-axis current cancellation [11]:* It shares the same strengths and limitations as pulsating *d-axis* current injection.

Due to its superior performance, pulsating *d*-axis high-frequency current injection will be considered hereafter.

If a pulsating *d*-axis high -frequency current is injected in the stator terminals of a PMSM (8), the resulting stator high-frequency voltage is given by (9). By taking the *d*-axis component of the high-frequency voltage complex vector, v^{r*}_{dqhf} in (9), a complex voltage vector $v^{r'}_{\mathrm{dqhf}}$, (10), can be defined. Both (8) and (10) can be separated into positive sequence ($i^{r'}_{\mathrm{dqhfpc}}$ and $v^{r'}_{\mathrm{dqhfpc}}$) and a negative sequence ($i^{r'}_{\mathrm{dqhfnc}}$ and $v^{r'}_{\mathrm{dqhfnc}}$) components (11)–(12), each of magnitude equal to half of that of the original signal. The *d*-axis impedance (13) can be obtained from (11) and (12) using either the positive or the negative sequence components (15), where φ_{Zd}, (14), is the phase of the *d*-axis PMSM high-frequency impedance (13)

$$i^{r*}_{\mathrm{dqhf}} = \begin{bmatrix} i^{r*}_{\mathrm{dhf}} \\ i^{r*}_{qhf} \end{bmatrix} = \begin{bmatrix} I^{*}_{hf}\cos\left(\omega_{hf}t\right) \\ 0 \end{bmatrix} \tag{8}$$

$$v^{r*}_{\mathrm{dqhf}} = \begin{bmatrix} v^{r*}_{\mathrm{dhf}} \\ v^{r*}_{\mathrm{qhf}} \end{bmatrix} = \begin{bmatrix} \left(R_{\mathrm{dhf}} + j\omega_{\mathrm{hf}}L_{\mathrm{dhf}}\right) i^{r}_{\mathrm{dhf}} \\ \omega_r L_{\mathrm{dhf}} \end{bmatrix} \tag{9}$$

$$v^{r'}_{dqhf} = \begin{bmatrix} v^{r*}_{dhf} \\ 0 \end{bmatrix} = \begin{bmatrix} \left(R_{dhf} + j\omega_{hf}L_{dhf}\right) I^{*}_{hf}\cos\left(\omega_{hf}t\right) \\ 0 \end{bmatrix}$$

$$= \begin{bmatrix} V^{r'}_{dqhf}\cos\left(\omega_{hf}t + \varphi_{Zd}\right) \\ 0 \end{bmatrix} \tag{10}$$

$$i^{r*}_{dqhf} = \frac{I_{hf}}{2}e^{j\omega_{hf}t} + \frac{I_{hf}}{2}e^{-j\omega_{hf}t} = i^{r*}_{dqhfpc} + i^{r*}_{dqhfnc} \tag{11}$$

$$v^{r'}_{dqhf} = \frac{\left|v^{r'}_{dqhf}\right|}{2}e^{j(\omega_{hf}t-\varphi_{Zd})} + \frac{\left|v^{r'}_{dqhf}\right|}{2}e^{j(-\omega_{hf}t+\varphi_{Zd})}$$

$$= v^{r'}_{dqhfpc} + v^{r'}_{dqhfnc} \tag{12}$$

$$Z_d = R_{\mathrm{dhf}} + j\omega_{\mathrm{hf}}L_{\mathrm{dhf}} \tag{13}$$

$$\varphi_{\mathrm{Zd}} = \tan^{-1}\left(\frac{\omega_{\mathrm{hf}}L_{\mathrm{dhf}}}{R_{\mathrm{dhf}}}\right) \tag{14}$$

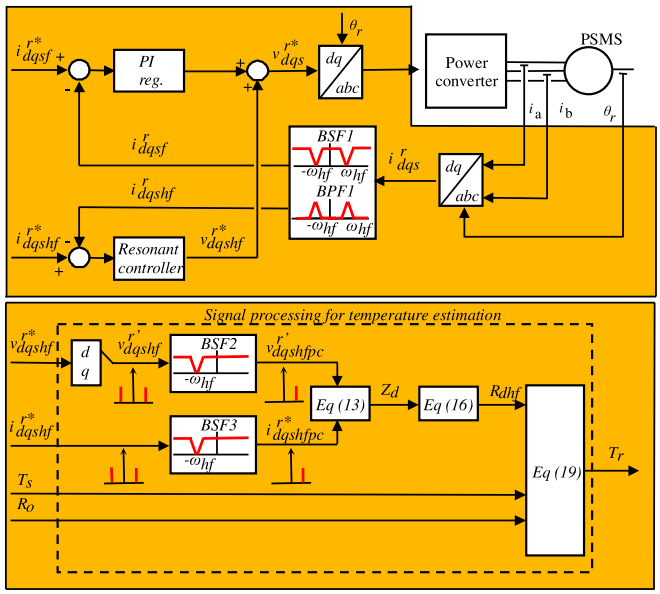

Fig. 2. Temperature estimation in a field oriented controlled ac drive using *d*-axis pulsating current injection, including power converter control (top) and signal processing (bottom).

$$Z_d = R_{\mathrm{dhf}} + j\omega_{\mathrm{hf}}L_{\mathrm{dhf}} = \frac{v^{r'}_{\mathrm{dqhfpc}}}{i^{r*}_{\mathrm{dqhfpc}}} = \frac{v^{r'}_{\mathrm{dqhfnc}}}{i^{r*}_{\mathrm{dqhfnc}}} \tag{15}$$

$$R_{\mathrm{dhf}} = Z_d\cos\left(\varphi_{\mathrm{Zd}}\right). \tag{16}$$

The overall *d-axis* high-frequency resistance (16) is split into the stator and rotor contributions $R_{\mathrm{dshf}(T_s)}$ and $R_{\mathrm{drhf}(T_r)}$ (17), which are function of the stator and rotor temperatures (T_s and T_r). The *d-axis* resistance can be expressed as (18), where α_{mag} is the magnet thermal resistive coefficient. The magnet temperature T_r can be finally obtained using (19)

$$R_{\mathrm{dhf}(T_s,T_r)} = R_{\mathrm{dshf}(T_s)} + R_{\mathrm{drhf}(T_r)} \tag{17}$$

$$R_{\mathrm{dhf}(T_s,T_r)} = R_{\mathrm{dshf}(T_0)}\left(1+\alpha_{\mathrm{cu}}\left(T_s - T_0\right)\right) + R_{\mathrm{drhf}(T_0)}\left(1+\alpha_{\mathrm{mag}}\left(T_r - T_0\right)\right) \tag{18}$$

$$T_r = \frac{R_{\mathrm{dhf}(T_s,T_r)} - R_{\mathrm{dshf}(T_0)}\left(1+\alpha_{\mathrm{cu}}\left(T_s - T_0\right)\right) - R_{\mathrm{drhf}(T_0)}}{R_{\mathrm{drhf}(T_0)}\alpha_{\mathrm{mag}}} + T_0. \tag{19}$$

Fig. 2 schematically shows the inverter control and signal processing needed for temperature estimation using *d-axis* pulsating high -frequency current injection. A band-stop filter (BSF1) is used in the current feedback to prevent the reaction of the fundamental current regulator against the injected high-frequency current, while a band-pass filter (BPF1) is used to isolate the positive and negative high-frequency current components (11).

The inputs to the temperature estimation block (see Fig. 2) are the output voltage of the high-frequency resonant current controller v^{r*}_{dqhf} (9), the commanded high -frequency current i^{r*}_{dqhf} (11), the measured stator temperature T_s, and the stator resistance at the room temperature R_0. Two band stop filters (BSF2 and BSF3 in Fig. 2) are used to remove the negative

sequence components. The magnet temperature is estimated using (19).

IV. Sensitivity Analysis

Though both BEMF and high-frequency signal injection methods use the same terminal electrical variables, there are significant differences in their parameter sensitivity and consequently in the expected accuracy. This issue is addressed following.

A. Sensitivity Analysis of BEMF Methods

BEMF methods are sensitive both to stator resistance variations as well as to inductance variations.

1) *Stator resistance ($R_{q(T_s)}$)*: sensitivity of $\lambda_{\mathrm{pm}(T_r)}$ to errors in the estimated stator resistance is given by

$$\frac{\partial \lambda_{\mathrm{pm}(T_r)}}{\partial R_{q(T_s)}} = \frac{i_q^r}{\omega_r}. \tag{20}$$

It is observed from (20) that the sensitivity increases with the q-axis current and decreases with the machine speed. Since BEMF methods are normally used in the high-speed region, the sensitivity to errors in the estimated stator resistance will be in general small.

2) *d-axis inductance ($L_{d(T_r,i_q^r,i_d^r)}$)*: sensitivity to d-axis inductance estimation is given by (21), and is equal to the d-axis current:

$$\frac{\partial \lambda_{\mathrm{pm}(T_r)}}{\partial L_{d\left(T_r,i_q^r,i_d^r\right)}} = i_d^r. \tag{21}$$

For SPMSMs operating below the base speed, the d-axis current is normally zero, increasing with the rotor speed in the flux-weakening region. On the contrary, the d-axis current is normally different from zero in IPMSMs uisng MTPA or other optimized strategies, independent of the speed. Consequently, for SPMSMs operating below their base speed, the method is not affected by errors in the estimated d-axis inductance; however, such errors must be considered when the machine operates above the base speed. For IPMSMs, the effect of *d-axis* inductance variation needs to be considered in the whole speed range. Comparing (20) and (21), it can be also concluded that the sensitivity of BEMF methods to d-axis inductance estimation errors will be in general larger than that to resistance estimation errors.

3) *q-axis inductance ($L_{q(T_r,i_q^r,i_d^r)}$)*: sensitivity to q-axis inductance estimation errors is given by

$$\frac{\partial \lambda_{\mathrm{pm}(T_r)}}{\partial L_{q\left(T_r,i_q^r,i_d^r\right)}} = \frac{1}{\omega_r}\frac{\partial i_q^r}{\partial t}. \tag{22}$$

It is observed that the sensitivity to q-axis inductance estimation errors will be zero in steady state operation. On the contrary, inadmissible estimation errors can occur if the estimation is realized during transients in the q-axis current, especially considering the high bandwidth typically used by the current regulators in ac drives.

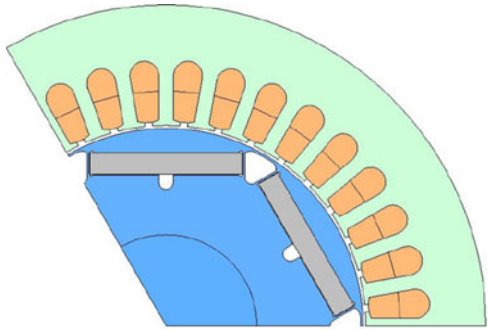

Fig. 3. IPMSM design.

TABLE II
Machine Parameters

P_{Rated} [kW]	V_{Rated} [V]	I_{Rated} [A]	ω_r [rpm]	Poles
7.5	350	14	1800	6

IPMSM.

B. Sensitivity of Pulsating d-Axis High-Frequency Current Injection Methods

Only the stator resistance affects to the estimated magnet temperature and needs, therefore, to be compensated for, when the pulsating *d-axis* high-frequency current is used for temperature estimation (17)–(19) [11]. The sensitivity of the estimated magnet temperature T_r to errors in the estimated d-axis high-frequency resistance is given by (23). It observed that the sensitivity is inversely proportional to the d-axis rotor high-frequency resistance at the room temperature $R_{\mathrm{drhf}(T_0)}$, and to the magnet thermal resistive coefficient α_{mag}, the sensitivity being, therefore, independent of the speed and I_d and I_q currents. It can be concluded that errors in the estimated d-axis high-frequency resistance will induce a constant temperature error, i.e., a dc offset in the estimated temperature

$$\frac{\partial T_r}{\partial R_{\mathrm{dhf}(T_s,T_r)}} = \frac{1}{R_{\mathrm{drhf}(T_0)}\alpha_{\mathrm{mag}}}. \tag{23}$$

V. Simulation Results

Finite element modeling (FEM) will be initially used for the verification of the conclusions reached in the previous section. Fig. 3 shows the machine design used for simulation, the parameters being shown in Table II. The same design will be used for the experimental verification.

A. BEMF -Based PM Temperature Estimation

As already mentioned, inductance maps are needed to estimate the PM flux from the BEMF (4). Fig. 4 shows the d- and q-axes inductance maps as a function of I_d and I_q for the test machine. As expected, I_d strongly affects to L_d while I_q strongly affects to L_q. A small coupling between the d- and q-axes is also observed.

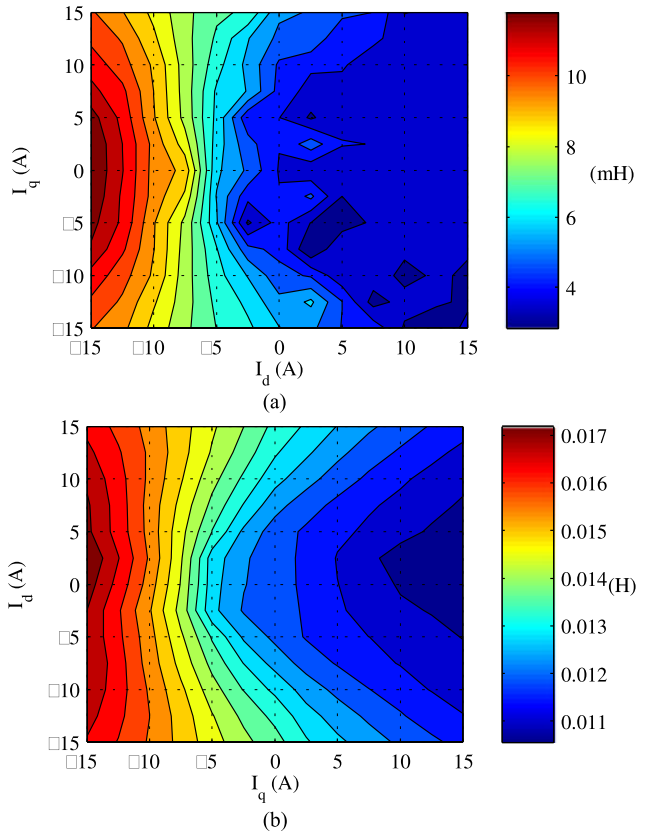

Fig. 4. FEM results. *D*- and *q*-axis inductance maps as a function of the *d*- and *q*-axes currents. (a) L_d and $(b) L_q$. $T_r = 20$ ºC.

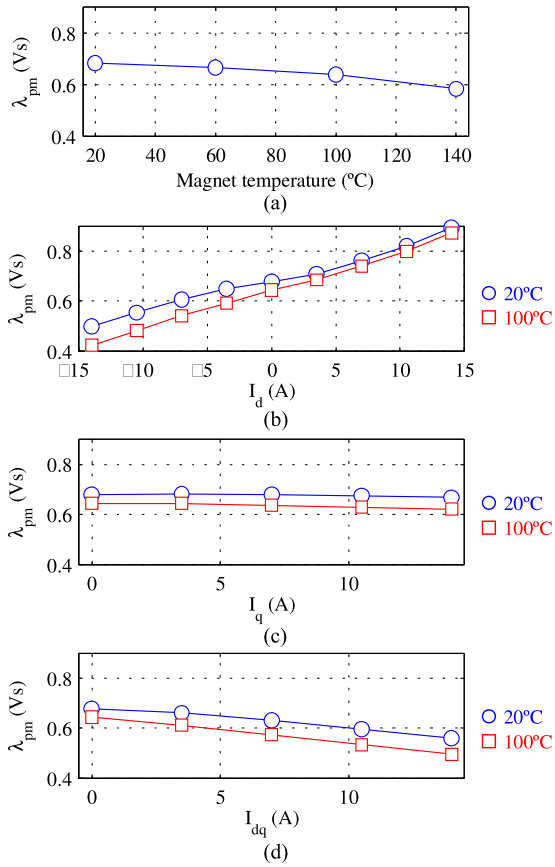

Fig. 5. PM flux ($\lambda_{\rm pm}$) versus (a) magnet temperature ($I_d = I_q = 0$), (b) I_d current, (c) I_q current, and (d) $I_{\rm dq}$ with -$I_d = I_q$. In all the cases, $\omega_r = 1$ p.u. Plots 5b, 5c, and 5d show the results for two different temperatures of 20 ºC and 100 ºC.

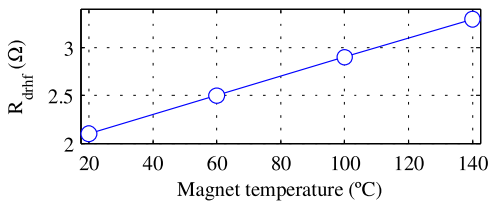

Fig. 6. Estimated rotor high-frequency resistance ($R_{\rm drhf}$) variation versus magnet temperature. Pulsating *d-axis* current injection. $\omega_{\rm hf} = 2 \cdot \pi \cdot 250$ rad/s and $I_{\rm hf} = 0.05$ p.u., $\omega_r = 1$ p.u.

Fig. 5(a) shows the PM flux as a function of the PM temperature. As expected, an almost linear relationship exits, meaning the estimation of the magnet temperature from the estimation PM flux linkage is expected to be straightforward.

As already mentioned, $\lambda_{\rm pm}$ also changes with I_d. Fig. 5(b) shows the variation of $\lambda_{\rm pm}$ when I_d changes from -1 to 1 p.u., for two different magnet temperatures of 20 ºC and 100 ºC. The change of $\lambda_{\rm pm}$ with I_d is seen to be smooth but nonlinear.

Similarly, Fig. 5(c) shows the variation of $\lambda_{\rm pm}$ with I_q for two different PM temperatures. The effect of I_q on $\lambda_{\rm pm}$ is seen to be significantly less relevant compared to the effect of I_d.

Finally, Fig. 5(d) shows the variation of $\lambda_{\rm pm}$ with the magnitude of the stator current vector for the case of $I_{\rm dq}$, $-I_d = I_q$ ($\beta = -45°$). As expected, the overall effects can be predicted from the combined effects of I_d and I_q.

It is concluded from the previous analysis that estimating the magnet temperature from $\lambda_{\rm pm}$ is not straightforward, some type of nonlinear function or lookup tables being needed to compensate the effects of I_d and I_q on $\lambda_{\rm pm}$.

B. Pulsating d-Axis High-Frequency Current Injection-Based PM Temperature Estimation

Fig. 6 shows the estimated rotor high-frequency resistance, $R_{{\rm drhf}(T_r)}$ (18), as a function of the PM temperature. A linear relationship of $\alpha_{\rm mag}$ is observed. No lookup tables or decoupling functions are, therefore, needed in this case, which is an advantage compared to BEMF methods.

VI. Experimental Results

Experimental tests have been conducted on the IPMSM shown in Fig. 7(a). Machine design and parameters are the same as for simulation (see Fig. 3 and Table II). The IPMSM is equipped with 13 thermocouples located along one PM [see Fig. 7(b)]. The average of the temperature provided by the 13 sensors will be used as the base temperature to evaluate the accuracy of both methods. The stator temperature was measured using a PT-100 temperature sensor. All the experimental results presented in this section were obtained with the machine

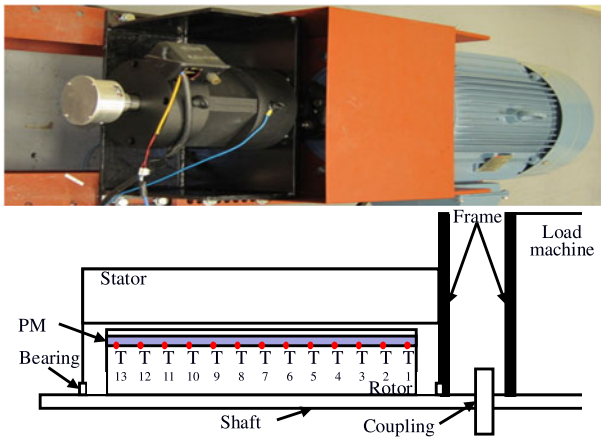

Fig. 7. (a) Experimental test bench (IPMSM) and (b) thermocouples location.

operating in steady state. For each operating condition, the temperature is measured 30 min. after the current $I_{\rm dq}$ is injected. This time was found to be enough for the machine to reach its steady-state thermal condition. The signal processing required for the estimation of the magnet temperature consumes ≤5 ms, which can considered negligible compared to the machine thermal time constant.

Fig. 8 shows the measured stator [see Fig. 8(a)] and magnet [see Fig. 8(b)] temperatures for different values of the speed and torque.. The operating points of the machine cover from zero to the corresponding speed and torque rated values in steps of 0.1 p.u. It is observed that the machine temperature increases with the speed, see Fig. 8(a) and (b), due to the increase of the eddy-current and hysteresis losses with frequency. The most critical working condition (higher temperatures) occurs at high speeds, in the flux-weakening region.

Fig. 8(c) shows the magnet temperature estimation error when using a pulsating *d-axis* high -frequency current injection. It is observed that the maximum estimation error is approximately 2.5 ºC, occurring in the low-torque, high-speed (flux weakening) region. Fig. 8(d) shows the magnet temperature estimation error when a 0.1 p.u. error is introduced in the estimated *d*-axis high-frequency resistance (pulsating *d-axis* high-frequency current injection being used). As predicted by (23), this induces a constant (dc offset) temperature error, the maximum estimation error increasing to approximately 6.1 ºC.

Fig. 8(e) shows the magnet temperature estimation error when the BEMF is used, L_d and L_q contours shown in Fig. 4, where used to estimate $\lambda_{\rm pm}$. Contrary to the pulsating *d-axis* high-frequency current injection method, the maximum temperature estimation error occurs in the low-speed region, i.e., when the speed is below approximately 0.1 p.u., due to the reduced BEMF. The estimation error is seen to decreas quickly as the speed increases, the estimation error being smaller than approximately 2.5 ºC for speeds >0.45 p.u.

Fig. 8(f)–(h) shows the magnet temperature estimation error when the BEMF is used for different errors in the model. Fig. 8(f) shows the magnet temperature estimation error when a 0.1 p.u. error is introduced in the estimated stator resistance. As predicted by (20), the sensitivity to the stator resistance is in general low; no significant differences are observed between Fig. 8(e) and (f). For values of the speed $\omega_r > 0.4$ pu, the maximum estimation error is approximately 2.58 ºC.

Fig. 8(g) shows the magnet temperature estimation error when a 0.1 p.u. error is introduced in the estimated *d*-axis inductance. As predicted by (21), the estimation error is proportional to I_d. MTPA is not implemented, i.e., $I_d = 0$ for $\omega_r < 1$ pu and $I_d \neq 0$ for $\omega_r > 1$ pu. The reason for not using MTPA with the IPMSM is to analyze the effects of changes in I_q, I_d, and ω_r separately. As expected, the maximum estimation error, approximately 5.8 ºC, occurs in the high-speed (high flux weakening) region.

Finally, Fig. 8(h) shows the magnet temperature estimation error when a 0.1 p.u. error is introduced in the estimated *q*-axis inductance. As the measurement are made with the machine operating in steady state, i.e., $pi_q^r = pi_d^r = 0$, the sensitivity to L_d estimation errors is zero. Due to this, no significant differences between Fig. 8(e) and (h) are observed.

VII. Combined Used of High-Frequency Signal Injection and BEMF-Based Methods

The results shown in Fig. 8(b) and (c) suggest that combined use of pulsating *d-axis* high-frequency signal injection and BEMF methods can provide increase accuracy and reduced parameter sensitivity. Pulsating *d-axis* high-frequency signal injection would be used in the low-speed range (e.g., $\omega_r < 0.4$ p.u.), while BEMF would be used in the mid-to-high speed region (e.g., $\omega_r > 0.6$ pu). A combination of both methods can be used in the transition region. It is noted in this regards that although in the mid-to-high speed range both methods provide similar accuracy, BEMF would be preferred, as it does not require the injection of test signal.

Fig. 9 shows the implementation when high-frequency signal injection and BEMF are combined. For $\omega_r < 0.4$ p.u. (see Fig. 9), i.e., low-speed region, only the high-frequency signal injection method is being used, as its accuracy is clearly superior than the BEMF-based method. For $\omega_r > 0.6$ p.u. (see Fig. 9), i.e., in the mid-to-high speed region, only the BEMF-based method is being used. For $0.4 < \omega_r < 0.6$ p.u., (25) (see Fig. 9), there is a linear transition between high-frequency signal injection and the BEMF. Fig. 10(a) shows the magnet temperature estimation error combining BEMF and high-frequency signal injection methods. The maximum temperature estimation error is approximately 2.7 ºC, which occurs in the transition region between both methods.

Finally, Fig. 10(b) shows the magnet temperature estimation error when there is a 0.1 p.u. error *d*-axis high-frequency resistance ($R_{\rm dhf(T_s,T_r)}$), *q*-axis resistance ($R_{q(T_s)}$), *d*-axis inductance ($L_{d(T_r,i_q^r,i_d^r)}$), and *q*-axis inductance ($L_{q(T_r,i_q^r,i_d^r)}$). It can be observed from Fig. 10(b) that the error corresponds to the combined effect of the errors observed in Fig. 8(d) and (f)–(h). The maximum estimation error is approximately 5.8 ºC, and occurs in the low-torque high-speed (high flux weakening) region due to the sensitivity of the BEMF method to the *d*-axis inductance variation.

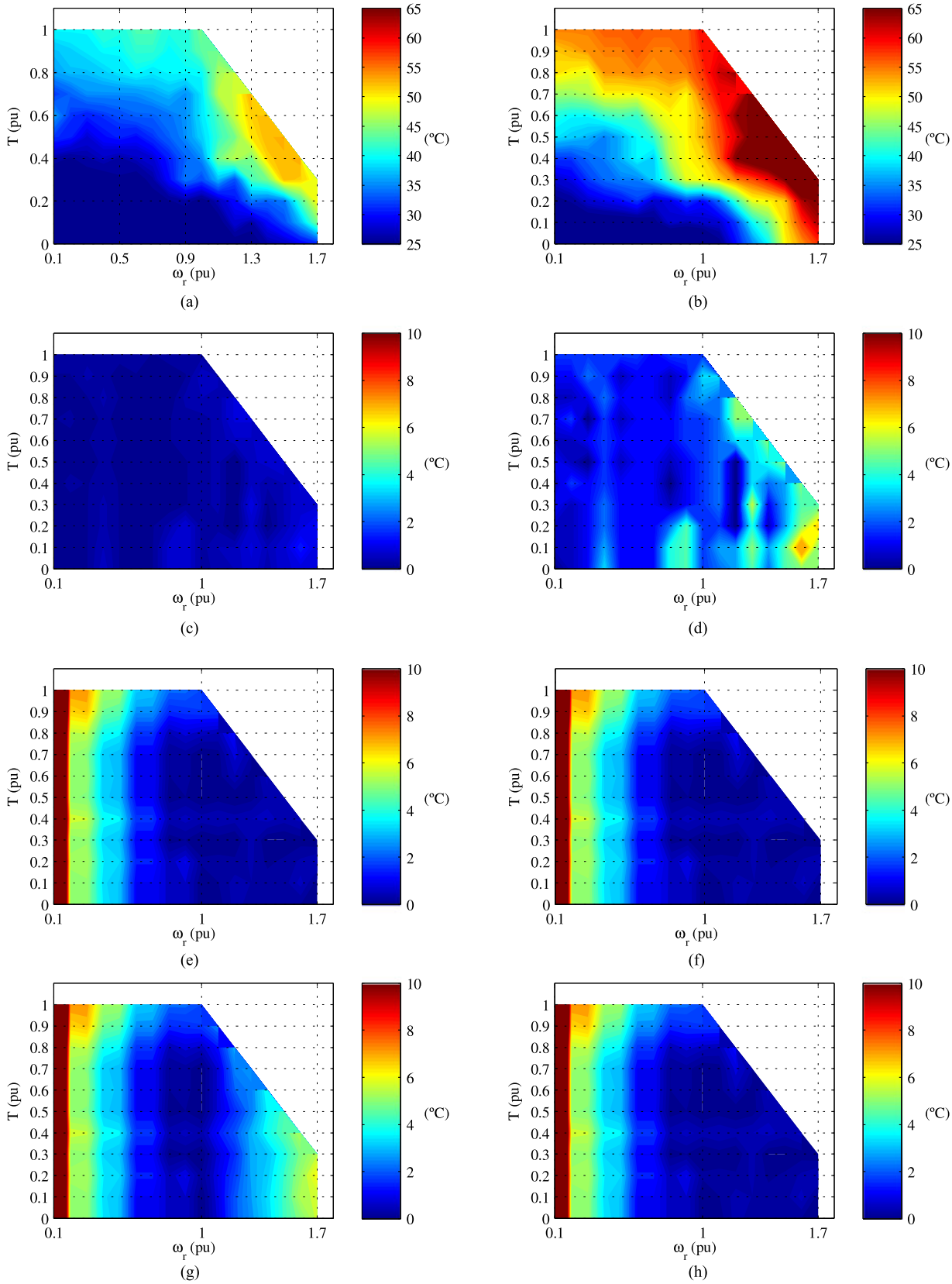

Fig. 8. Experimental results. Measured stator and rotor temperatures and magnet temperature estimation errors as a function of speed and torque. (a) Stator and (b) rotor temperatures. (c) Magnet temperature estimation error using *d*-axis pulsating high-frequency signal injection without parameter estimation error, (d) error when a 0.1 p.u. error is introduced in the estimated *d*-axis high-frequency resistance. $\omega_{\mathrm{hf}} = 2 * \pi * 250$ Hz, $V_{\mathrm{hf}} = 0.1$ p.u. and $I_{\mathrm{hf}} = 0.05$ p.u. (e) Magnet temperature estimation error using the BEMF without parameter estimation error, (f) the same introducing a 0.1 p.u. error in the estimated *d*-axis resistance, (g) the same introducing a 0.1 p.u. error in the estimated *d*-axis inductance, and (h) the same introducing a 0.1 p.u. error in the estimated *q*-axis inductance.

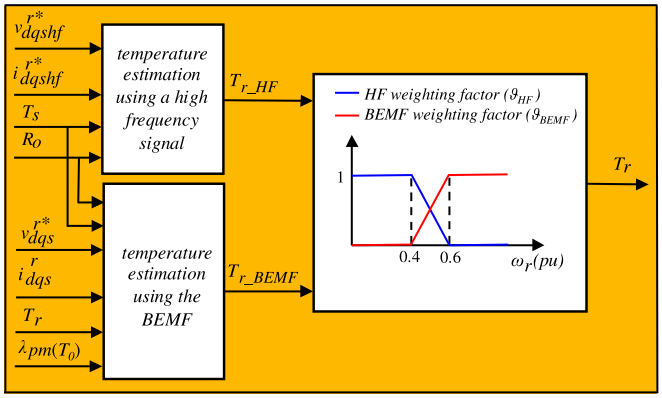

Fig. 9. Signal processing for the combined use of high-frequency signal injection and BEMF.

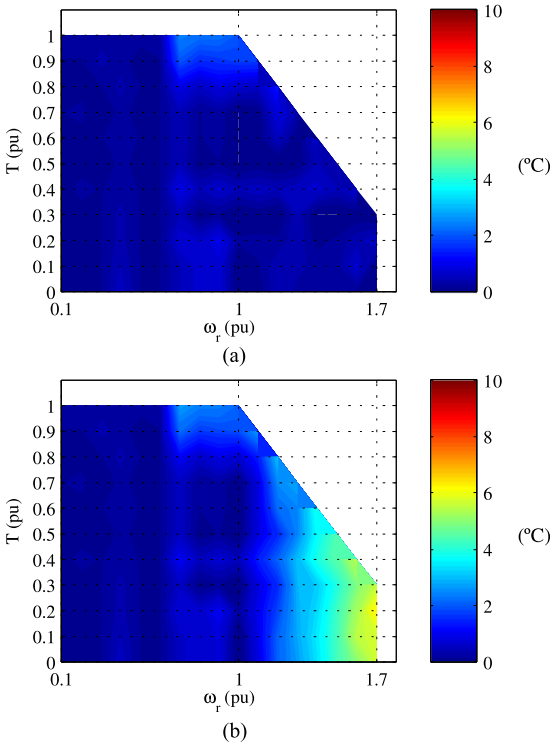

Fig. 10. Experimentally magnet temperature estimation errors when combing the pulsating *d-axis* high-frequency signal and the BEMF without introducing parameter estimation errors (a) and (b) introducing parameter estimation errors: 0.1 p.u. error in the estimated *d*-axis high-frequency resistance, in the estimated *d*-axis resistance, in the estimated *d*-axis inductance, and in the estimated *q*-axis inductance. $\omega_{\rm hf} = 2 * \pi * 250$ Hz and $I_{\rm hf} = 0.05$ p.u.

VIII. Conclusion

Comparative analysis of BEMF and pulsating *d*-axis high-frequency current injection methods for magnet temperature estimation in PMSMs is presented in this paper. Parameter sensitivity analysis for both methods has been provided. It has been shown that the *d*-axis pulsating high-frequency current injection can potentially provide higher performance compared to BEMF, due to its reduced parameter sensitivity and its capability to operate in the low-speed region. However, BEMF-based methods exhibit an excellent performance in the mid-to-high-speed region and does not require the injection of a test signal. Combined use of both methods is, therefore, a viable and promising alternative. Experimental results that confirm the concepts discussed in this paper have been provided.

References

[1] J. F. Gieras and M. Wing, *Permanent Magnet Motor Technology: Design and Application*, 2nd ed. Boca Raton, FL, USA: CRC Press, 2002.

[2] N. Limsuwan, Y. Shibukawa, D. Reigosa, M. Leetmaa and R. D. Lorenz, "Novel design of flux-intensifying interior permanent magnet synchronous machine suitable for power conversion and self-sensing control at very low speed," *IEEE Trans. Ind. Appl.*, vol. 47 no. 5 pp. 2004–2012, Sep./Oct. 2011.

[3] D. Reigosa, K. Akatsu, N. Limsuwan, Y. Shibukawa and R. D. Lorenz, "Self-sensing comparison of fractional slot pitch winding versus distributed winding for FW- and FI-ipmsms based on carrier signal injection at very low speed," *IEEE Trans. Ind. Appl.*, vol. 46, no. 6, pp. 2467–2474, Nov./Dec. 2010.

[4] K. Akatsu and S. Wakui, "Torque and power density comparison between fractional-slot concentrated winding SPMSMs," presented at the Int. Conf. Elect. Mach. Syst., CD-ROM, Nagasaki, Japan, Nov. 2006.

[5] K. Akatsu, K. Narita, Y. Sakashita, and T. Yamada, "Characteristics comparison between SPMSM and IPMSM based on both analytical and experimental results," in presented at the Int. Conf. Elect. Mach. Syst., CD-ROM, Wuhan, China, Oct. 2008.

[6] S. Wu *et al.*, "IPM synchronous motor design for improving self-sensing performance at very low speed", *IEEE Trans. Ind. Appl.*, vol. 45 no. 6, pp. 1939–1946, Nov./Dec. 2009.

[7] N. Bianchi and T. M. Jahns, "Design, analysis, and control of interior pm synchronous machines," *Tutorial Course Notes* presented at the IEEE Ind. Appl. Soc. Meeting, Seattle, WA, USA, Oct. 2004.

[8] D. Reigosa, F. Briz, P. García, J. M. Guerrero, and M. W. Degner, "Magnet temperature estimation in surface PM machines using high frequency signal injection," *IEEE Trans. Ind. Appl.*, vol. 46 no. 4, pp. 1468–1475, Jul./Aug. 2010.

[9] D. Reigosa, F. Briz, M. W. Degner, P. García, and J. M. Guerrero, "Magnet temperature estimation in surface PM machines during six-step operation," *IEEE Trans. Ind. Appl.*, vol. 48 no. 6, pp. 2353–2361, Nov./Dec. 2012.

[10] D. Reigosa, F. Briz, M. W. Degner, P. García, and J. M. Guerrero, "Temperature issues in saliency-tracking-based sensorless methods for PM synchronous machines," *IEEE Trans. Ind. Appl.*, vol. 47 no. 3, pp. 1352–1360, May/Jun. 2011.

[11] D. Reigosa, D. Fernandez, H. Yoshida, T. Kato, and F. Briz "Permanent magnet temperature estimation in PMSMs using pulsating high frequency current injection," in *Proc. IEEE Energy Convers. Congr. Expo.*, Sep. 2014, pp. 1729–1736.

[12] M. Kamiya, Y. Kawase, Y. Kosada, and N. Matsui, "Temperature distribution analysis of permanent magnet in interior permanent magnet synchronous motor considering PWM carrier harmonics," in *Proc. IEEE Int. Conf. Elect. Mach. Syst.*, Oct. 2007, pp. 2023–2027.

[13] P. Milanfar and J. H. Lang, "Monitoring the thermal condition of permanent-magnet synchronous motors," *IEEE Trans. Aerosp. Electron. Syst.*, vol. 32 no. 4, pp. 1421–1429, Oct. 1996.

[14] M Ganchev, C. Kral, and T. Wolbank, "Compensation of speed dependency in sensorless rotor temperature estimation for permanent-magnet synchronous motors," *IEEE Trans. Ind. Appl.*, vol. 49 no. 6, pp. 2487–2495, Nov./Dec. 2013.

[15] K. Liu and Z. Q. Zhu "Online estimation of the rotor flux linkage and voltage-source inverter nonlinearity in permanent magnet synchronous machine drives," *IEEE Trans. Power Electron.*, vol. 29 no. 1, pp. 418–427, Jan. 2014.

[16] K. Liu and Z. Q. Zhu "Mechanical parameter estimation of permanent magnet synchronous machines with aiding from estimation of rotor PM flux linkage," in *Proc. IEEE Energy Convers. Congr. Expo.*, Sep. 2014, pp. 4850–4857.

[17] S. Underwood and I. Husain, "On-line parameter estimation and adaptive control of permanent magnet synchronous machines," *IEEE Trans. Ind. Electr.*, vol. 57 no. 7, pp. 2435–2443, Jun. 2010.

[18] S. Ichikawa, M. Tomita, S. Doki, and S. Okuma, "Sensorless control of permanent-magnet synchronous motors using online parameter identification based on system identification theory," *IEEE Trans. Ind. Electron.*, vol. 53, no. 2, pp. 363–372, Apr. 2006.

David Reigosa (S'03-M'07) was born in Spain, in 1979. He received the M.E. and Ph.D. degrees in electrical engineering from the University of Oviedo, Gijon, Spain, in 2003 and 2007, respectively. From 2004 to 2008, he was awarded and fellowship of the Personnel Research Training Program funded by Regional Ministry of Education and Science of the Principality of Asturias. He was a Visitor Scholar at the Wisconsin Electric Machines and Power Electronics Consortium, University of Wisconsin, Madison, WI, USA, in 2007.

He is currently an Associate Professor in the Department of Electrical Engineering, University of Oviedo. His research interests include sensorless control of induction motors, permanent magnet synchronous motors, and digital signal processing.

Daniel Fernandez was born in Spain, in 1987. He received the B.S degree in industrial electronic engineering, in 2011, and the M.S. degree in power electronic engineering, in 2013, from the University of Oviedo, Gijon, Spain, where he is currently working toward the Ph.D. degree in electrical engineering.

From July 2013 to December 2013, he was an Intern at the Nissan Advanced Technology Center. His research interests include electric motors and drives, magnets, and wireless measurement systems. He received a fellowship of the Personnel Research Training Program funded by the Regional Ministry of Education and Science of the Principality of Asturias in 2013.

Tsutomu Tanimoto received the B.S. degree in electrical engineering from the Tokyo University of Science, Chiba, Japan, in 1999.

He joined AISIN AW Company Ltd., Aichi, Japan in 1999, he contributed to the control of electric machines. In 2002, he joined Nissan Research Center, Yokosuka, Japan, where he contributed to the design and control of switched reluctance machines and permanent magnet machines. He is currently with the Electric Vehicle System Laboratory, Nissan Motor Company Ltd., Atsugi, Japan. His research interests include electric motor design and control. He is a Member of the Institute of Electrical Engineers of Japan.

Takashi Kato received the B.S. degree in mechanical system engineering from Kansai University, Osaka, Japan, in 1997, and the Ph.D. degree from Shibaura Institute of technology, Tokyo, Japan, in 2015.

He joined the Nissan Research Center in 2001. He has contributed to the electric machine design and control. He was a Visiting Researcher in the Wisconsin Electric Machines and Power Electronics Consortium, at University of Wisconsin Madison, Madison, WI, USA, from 2010 to 2012. His research interests are electric motor design and control.

Dr. Kato is a Member of the IEE of Japan and the Japan Society of Mechanical Engineers.

Fernando Briz (A'96–M'99–SM'06) received the M.S. and Ph.D. degrees from the University of Oviedo, Gijón, Spain, in 1990 and 1996, respectively.

He is currently a Full Professor with the Department of Electrical, Computer and Systems Engineering, University of Oviedo. His topics of interest include electronic power converters and ac drives, power systems, machine monitoring and diagnostics and digital signal processing.

Dr. Briz received the 2005 IEEE TRANSACTIONS ON INDUSTRY APPLICATIONS Third Place Prize Paper Award and receivd seven IEEE Industry Applications Society Conference and IEEE Energy Conversion Congress and Exposition Prize Paper Awards. He is currently the Publications Chair and an Associate Editor of the Industrial Drives Committee of the IAS-IPCSD.